Research Article Vol. 24, No. 19 | 5 Sep 2016 | OPTICS EXPRESS 22034

Optics EXPRESS

Analysis and reduction of errors caused by Poisson noise for phase diversity technique

HONGLI YU,[1,2] CHENGLIANG YANG,[1,3] ZIHAO XU,[1,2] PEIGUANG ZHANG,[1] HUANYU XU,[1] ZHAOLIANG CAO,[1] QUANQUAN MU,[1,4] AND LI XUAN[1]

[1]*State Key Laboratory of Applied Optics, Changchun Institute of Optics, Fine Mechanics and Physics, Chinese Academy of Sciences, 130033, Changchun, Jilin, China*
[2]*Graduate School of the Chinese Academy of Science, Beijing 100039, China*
[3]*ycldahai@ciomp.ac.cn*
[4]*muquanquan@ciomp.ac.cn*

Abstract: An effective method for reducing the sensitivity of phase diversity (PD) technique to Poisson noise is proposed. The denoising algorithm based on blocking-matching and 3D filtering is first introduced in the wavefront sensing field as a preprocessing stage. Then, the PD technique is applied to the denoised images. Results of the numerical simulations and experiments demonstrate that our approach is better than the traditional PD technique in terms of both the root-mean-square error (RMSE) of phase estimates and the structural similarity index metrics (SSIM). The RMSEs of phase estimates on synthetic data are decreased by approximately 40% across noise levels within the range of 58.7-18.8 dB in terms of peak signal-to-noise ratio (PSNR). Meanwhile, the overall decline range of SSIM is significantly decreased from 49% to 9%. The experiment and simulation results are in good agreement. The approach may be widely used in various domains, such as the measurements of intrinsic aberrations in optical systems and compensations for atmospheric turbulence.

OCIS codes: (010.7350) Wave-front sensing; (100.2000) Digital image processing; (100.3010) Image reconstruction techniques; (100.5070) Phase retrieval.

References and links

1. R. A. Gonsalves and R. Chidlaw, "Wavefront sensing by phase retrieval," Proc. SPIE **0207**, 32–39 (1979).
2. R. A. Gonsalves, "Phase retrieval and diversity in adaptive optics," Opt. Eng. **21**(5), 215829 (1982).
3. R. G. Paxman, T. J. Schulz, and J. R. Fienup, "Joint estimation of object and aberrations by using phase diversity," J. Opt. Soc. Am. A **9**(7), 1072–1085 (1992).
4. J. J. Dolne, "Evaluation of the phase diversity algorithm for noise statistics error and diversity function combination," Proc. SPIE **6307**, 630708 (2006).
5. R. L. Kendrick, D. S. Acton, and A. L. Duncan, "Phase-diversity wave-front sensor for imaging systems," Appl. Opt. **33**(27), 6533–6546 (1994).
6. B. L. Ellerbroek, B. J. Thelen, D. J. Lee, D. A. Carrara, and R. G. Paxman, "Comparison of Shack-Hartmann wavefront sensing and phase-diverse phase retrieval," Proc. SPIE **3126**, 3126307 (1997).
7. J. H. Seldin and R. G. Paxman, "Phase-diverse speckle reconstruction of solar data," Proc. SPIE **2302**, 2302268 (1994).
8. M. G. Löfdahl and G. B. Scharmer, "Application of phase-diversity to solar images," Proc. SPIE **2302**, 2302254 (1994).
9. M. G. Löfdahl, R. L. Kendrick, A. Harwit, K. E. Mitchell, A. L. Duncan, J. H. Seldin, R. G. Paxman, and D. S. Acton, "Phase diversity experiment to measure piston misalignment on the segmented primary mirror of the Keck II Telescope," Proc. SPIE **3356**, 33561190 (1998).
10. L. Meynadier, V. Michau, M. T. Velluet, J. M. Conan, L. M. Mugnier, and G. Rousset, "Noise propagation in wave-front sensing with phase diversity," Appl. Opt. **38**(23), 4967–4979 (1999).
11. J. W. Goodman, *Introduction to Fourier Optics* (McGraw-Hill, 1968).
12. R. J. Noll, "Zernike polynomials and atmospheric turbulence," J. Opt. Soc. Am. **66**(3), 207–211 (1976).
13. K. Dabov, A. Foi, V. Katkovnik, and K. Egiazarian, "Image denoising by sparse 3-D transform-domain collaborative filtering," IEEE Trans. Image Process. **16**(8), 2080–2095 (2007).
14. K. Dabov, A. Foi, V. Katkovnik, and K. Egiazarian, "Image denoising with block-matching and 3D filtering," Proc. SPIE **6064**, 606414 (2006).
15. M. Mäkitalo and A. Foi, "Optimal inversion of the Anscombe transformation in low-count Poisson image denoising," IEEE Trans. Image Process. **20**(1), 99–109 (2011).
16. D. J. Lee, M. C. Roggemann, and B. M. Welsh, "Cramér-Rao analysis of phase-diverse wave-front sensing," J.

#270257 http://dx.doi.org/10.1364/OE.24.022034
Journal © 2016 Received 11 Jul 2016; revised 29 Aug 2016; accepted 31 Aug 2016; published 13 Sep 2016

Optics EXPRESS

Opt. Soc. Am. A **16**(5), 1005–1015 (1999).

17. J. J. Dolne, R. J. Tansey, K. A. Black, J. H. Deville, P. R. Cunningham, K. C. Widen, and P. S. Idell, "Practical issues in wave-front sensing by use of phase diversity," Appl. Opt. **42**(26), 5284–5289 (2003).
18. M. G. Löfdahl and G. B. Scharmer, "Wave-front sensing and image restoration from focused and defocused solar images," Astrophys. Suppl. Ser. **107**, 243–264 (1994).
19. V. N. Mahajan, "Strehl ratio for primary aberrations in terms of their aberration variance," J. Opt. Soc. Am. **72**, 1258–1266 (1982).

1. Introduction

The phase diversity technique, which was first proposed by Gonsalves in 1979, has since developed to have an important role in active and adaptive optic systems [1, 2]. This technique is used to simultaneously infer phase aberrations and reconstruct an object from two or more degraded images of the same object. A known phase diversity is introduced between these images, with defocusing as the most common approach. Paxman et al first derived the expressions for an aberration-only objective function that accommodated an arbitrary number of diversity images in 1992 [3]. The effect of phase diversity function combination on residual wavefront error was explicitly analyzed by Dolne in 2005 [4]. Unlike traditional wavefront sensors, the PD technique offers several advantages, such as no special requirement for optical hardware, feasibility of both point source and extended objects, and does not require any calibration [5, 6]. The PD technique was applied to solar imaging by Seldin et al to overcome the effects of atmospheric turbulence and to restore a fine-resolution image of solar granulation [7, 8]. The piston error of the Keck II Telescope was precisely measured using the PD technique [9]. However, noise data are inevitably recorded, thereby leading to the loss of image details and reduced contrast. The imaging process is based on photon detection; thus, Poisson noise is a predominant noise source in various domains, such as in astronomical observation and medical imaging. Essential information buried in Poisson noise reduces the estimation precision of phase aberrations and deteriorates the quality of reconstructed images for the PD technique, particularly at low light levels [10]. For example, astronomers like to observe faint stars at low magnitudes, that is, faint sources or large distance conditions are popular in adaptive optic systems. Consequently, improving the PD technique is imperative to ensure that it will remain effective in systems with massive Poisson noise.

In this study, we propose an effective approach to reduce the sensitivity of the traditional PD technique to Poisson noise. The approach is tested both on numerically simulated data and experimentally recorded images. The results show an improved performance across different noise levels. The accuracy of the estimated phase aberrations on synthetic data improves as calculated using the RMSE. The RMSEs of the phase estimates in the case of the improved PD are approximately 40% lower than that in the case of the traditional PD under each noise strength level ranging from 58.7 dB to 18.8 dB. The quality of the reconstructed images also considerably improves as evaluated visually and as calculated using the SSIM. The subjective visual quality is apparently improved given that the remaining amount of grains is minimal, and details are well-preserved. The SSIM for the improved PD deceases gradually and its overall decline range is less than 9%. By contrast, the SSIM for the traditional PD decreases dramatically and drops by over 49%. The results of the subjective visual quality and SSIM obtained via experiments are in good agreement with the simulation results.

2. Principles

PD is known to simultaneously estimate phase aberrations and reconstruct an object from two or more images. One of these images is the conventional focal-plane image that is degraded by unknown aberrations, and intentional phase diversities are introduced into the other images. The phase diversity used in this paper is defocus, which is the most commonly considered approach.

Optics EXPRESS

For a space-invariant incoherent imaging system, the image can be described as a convolution between the pristine object f and the point spread function (PSF) $s(x)$ as follows:

$$g_k(x) = f * s_k(x), \tag{1}$$

where x is the spatial coordinate, $*$ stands for the convolution operation, $s_k(x)$ is a PSF with diversity k, and g_k is the kth diversity image [11]. The PSF $s_k(x)$ is described as follows:

$$s_k(x) = \left| F^{-1}\left\{ p e^{i(\phi_t + \theta_k)} \right\} \right|^2, \tag{2}$$

$$\phi_t = \sum_{j=1}^{J} \alpha_j \phi_j, \tag{3}$$

where F^{-1} represents the inverse Fourier transform; p is a binary pupil function with values of 1 inside the pupil and 0 outside it; θ_k is a known phase function; and ϕ_t is the unknown phase aberration function to be estimated, which can be expressed as a set of basis functions ϕ_j with coefficients α_j. The basis functions used in this study is Zernike polynomials [12].

Noise is recorded while the true object is obtained by detectors. The noise model is roughly regarded as additive white noise. Each detected diversity image $d_k(x)$ is described as follows:

$$d_k(x) = g_k(x) + n_k(x). \tag{4}$$

Maximum likelihood estimation theory mentions that the traditional objective function to be minimized and the object expression can be obtained after reducing the dimension of the parameter space as follows:

$$E(\alpha) = \sum_u \frac{\left| D_1(u) S_1(u) - D_2(u) S_2(u) \right|^2}{\left| S_1(u) \right|^2 + \left| S_2(u) \right|^2}, \tag{5}$$

$$F(u) = \frac{D_1(u) S_1^*(u) + D_2(u) S_2^*(u)}{\left| S_1(u) \right|^2 + \left| S_2(u) \right|^2}, \tag{6}$$

where D_k, F, and S_k are the discrete Fourier transforms of d_k, f, and s_k, respectively. The superscript $*$ indicates a complex conjugation [3].

As indicated in Eqs. (5) and (6), the calculated total image data consist not only of the object information but also of noise data. However, the noisy points randomly distributed in images do not satisfy the PD relationship between focused and defocused images. Consequently, the phase aberration accuracy estimated using Eq. (5) decreases significantly at high noise levels. The reconstructed object is also distorted by the original noise data. Therefore, the main objective of this work is to weaken the influence of Poisson noise on the PD technique.

In this study, a denoising strategy based on the blocking-matching and 3D filtering (BM3D) algorithm is first introduced into the PD technique. The realization of BM3D includes three major steps: grouping by matching, collaborative filtering by shrinkage in the transform domain, and aggregation [13–15]. First, similar 2D fragments of the image are grouped into 3D data arrays. Second, the collaborative transform-domain shrinkage includes three successive steps: applying 3D linear transform to the group, shrinking the transform coefficients to reduce noise, and applying inverse linear transform to produce estimates of all the grouped blocks. Third, the global estimate $\hat{y}^{final}$ is computed using a weighted average of the blockwise estimates $\hat{Y}_x^{x_R}$.

We propose an effective approach to improve the performance of the traditional PD used in adaptive or active systems with considerable Poisson noise. The denoising algorithm is applied to noisy focused and defocused images as a preprocessing stage. The global estimate $\hat{y}(x)$ of the noisy image is obtained. PD technique is applied to the denoised images to estimate phase aberrations and to reconstruct objects. Thus, the new error metric and object expression are transformed into

$$E(\alpha)=\sum_u \frac{\left|Y_1(u)S_1(u)-Y_2(u)S_2(u)\right|^2}{\left|S_1(u)\right|^2+\left|S_2(u)\right|^2}, \tag{7}$$

$$F(u)=\frac{Y_1(u)S_1^*(u)+Y_2(u)S_2^*(u)}{\left|S_1(u)\right|^2+\left|S_2(u)\right|^2}, \tag{8}$$

where $Y(u)$ is the discrete Fourier transform of $\hat{y}(x)$ obtained using the denoising algorithm. Particle swarm optimization is applied to the new error metric to estimate the aberration and the object.

3. Simulations and experiments

3.1 Simulations

The focused and defocused images are degraded by a known random phase aberration, which is expressed as a set of Zernike polynomials with different weights. According to some previous works [16–18], the defocus distance introduced in this study is 1 wavelength, peak-to-valley (PV). Poisson noise is added to the degraded images at several noise levels to simulate low light conditions. The original object used in this study, i.e., Peppers, is shown in Fig. 1(a). The random phase aberrations used in this study is illustrated in Fig. 1(b). The image is degraded using the same aberration form in three different root-mean-square (RMS) scales, namely, 0.0572 λ, 0.1327 λ, and 0.2006 λ, which are denoted by aberrations a, b, and c, respectively. The given phase aberration also can be indicated by the input Strehl Ratio (SR), which equals to 0.879, 0.499, and 0.204, respectively, as calculated by Eq. (9) [19].

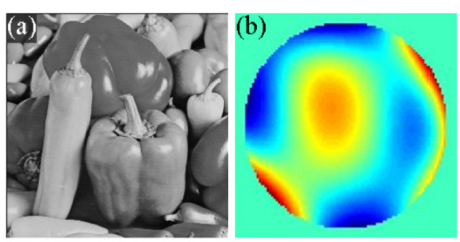

Fig. 1. (a) Original object and (b) known aberration form

$$SR \approx \exp[-(\frac{2\pi\sigma_w}{\lambda})^2]. \tag{9}$$

The noise level is indicated by PSNR of the degraded focused image. The accuracy of the estimated phase aberrations is evaluated using the RMSE of phase estimates. Moreover, SSIM is used as an objective evaluation of image quality. PSNR, RMSE, and SSIM are calculated as follows.

Optics EXPRESS

$$PSNR = 10\log_{10}\left(\frac{\max(d(j))^2}{\sum_{j=1}^{N}(d(j)-d_{noisy}(j))^2 / N}\right), \tag{10}$$

where $d(j)$ is the noiseless focused image, $d_{noisy}(j)$ is the noisy focused image, and N indicates the number of total pixels.

$$RMSE(\hat{\phi}) = \sqrt{\sum_{j=1}^{N_{pupil}}[\phi(j)-\hat{\phi}(j)]^2 / N_{pupil}}, \tag{11}$$

where $\phi(j)$ is the true phase aberration that is known in advance at coordinate j, $\hat{\phi}(j)$ is the estimated phase aberration, and N_{pupil} indicates the number of points in the discrete aperture.

$$SSIM(f,\hat{f}) = \frac{(2\mu_f\mu_{\hat{f}}+c_1)(2\sigma_{f,\hat{f}}+c_2)}{(\mu_f^2+\mu_{\hat{f}}^2+c_1)(\sigma_f^2+\sigma_{\hat{f}}^2+c_2)}, \tag{12}$$

where f is the pristine object, $\hat{f}$ refers to the estimated object, μ is the average, and σ^2 is the variance. The constants c_1 and c_2 are used to stabilize the division with a weak denominator.

Phase estimation accuracy is shown in the plots in Figs. 2(a), 2(c), and 2(e). The plots demonstrate an increasing tendency in terms of the RMSE of phase estimates as noise strength increases in both the improved and traditional PD cases. However, the RMSE in the improved PD case is consistently approximately 40% lower than that in the traditional PD case for all noise levels under each phase aberration. The results in terms of SSIM are shown in the plots in Figs. 2(b), 2(d), and 2(f). As the noise level increases, a sharp drop in SSIM is observed in the traditional PD case, in which SSIM decreases by 51.7%, 49.6%, and 58.2% for each aberration. By contrast, SSIM remains stable across different noise levels in the improved PD cases. The overall decline range is 8.2%, 7.8%, and 8.0% for each aberration. As shown in Fig. 3, the performance of the improved PD technique is also better than that of the traditional PD technique in terms of subjective visual perception at different noise levels for each phase aberration. At a high PSNR level of 58 dB, no evident difference is observed between the images reconstructed using the improved and traditional PD techniques. At a low PSNR level of 25 dB, the reconstructed images are distorted by numerous grains. By contrast, our approach achieves a considerably better performance in terms of visual perception because the remaining amount of grains is minimal, and the details are well-preserved. Therefore, the improved PD algorithm exhibits better performance on aberration estimation and image restoration at all noise levels compared with the traditional PD algorithm. In summary, the traditional PD technique is highly sensitive to noise and our approach can significantly improve the traditional PD technique across different noise levels.

Optics EXPRESS

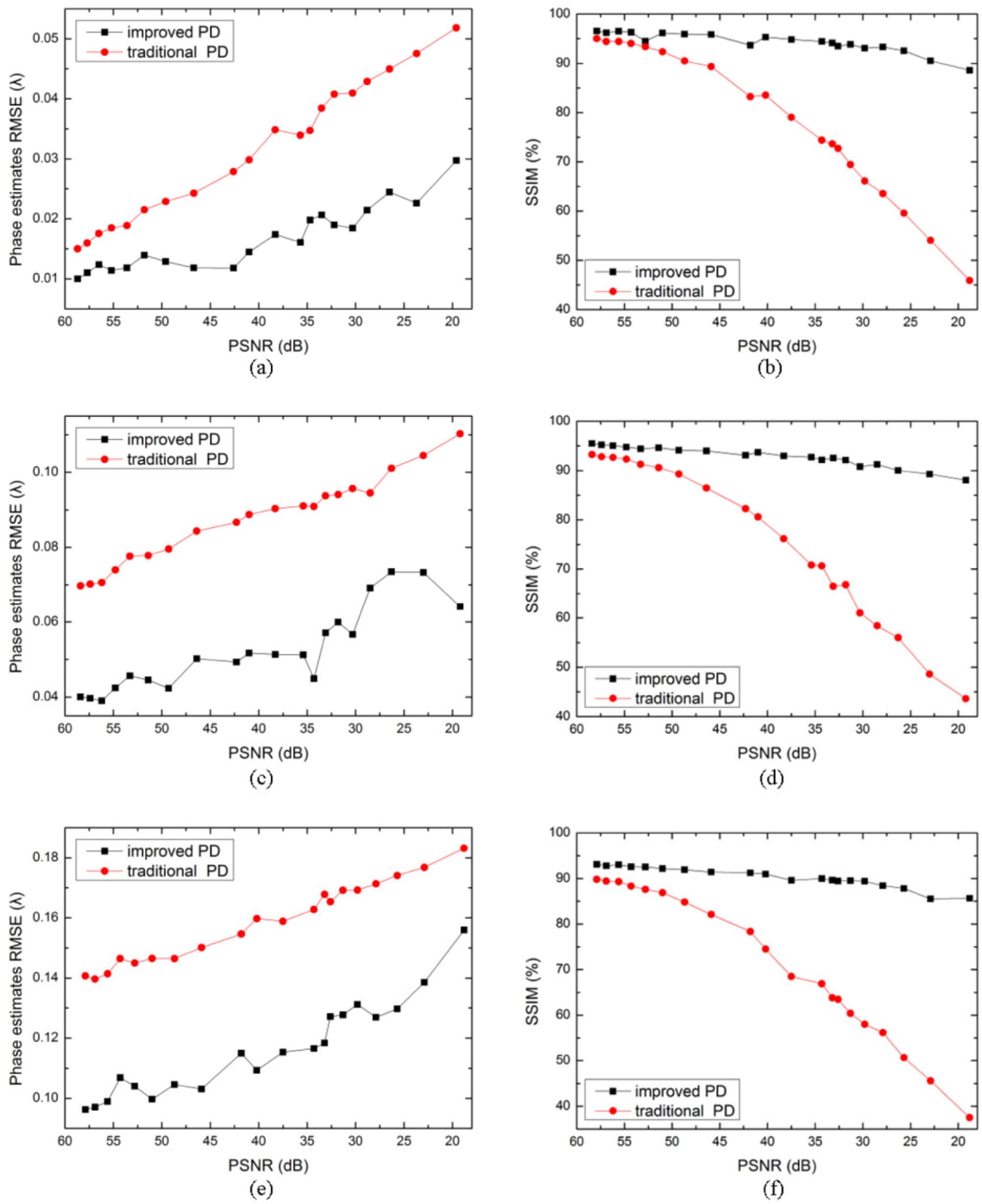

Fig. 2. Plots (a), (c), and (e): simulation results in terms of the RMSEs of phase estimates for aberrations a, b, and c, respectively. Plots (b), (d), and (f): simulation results in terms of SSIM. The RMSEs and SSIM are both as functions of the PSNR of the noisy focused image.

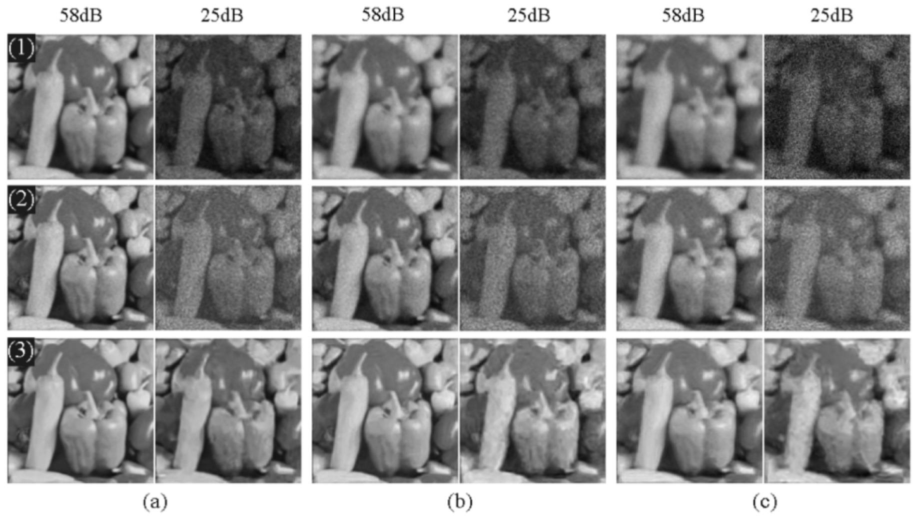

Fig. 3. Images for aberrations a, b, and c are denoted by (a), (b), and (c), respectively. Row 1: noisy focus-plane images degraded by aberrations at the PSNR levels of 58 dB and 25 dB. Row 2: reconstructed images using the traditional PD. Row 3: reconstructed images using the improved PD.

3.2 Experiments

The performance of the improved PD technique is demonstrated through a series of experiments, and the optical configuration is shown in Fig. 4. Lens L1 ($f = 105mm, \Phi = 25.4mm$) is used to collimate the light coming from the fiber. The collimated incident beam passes through a filter ($633nm$) and a beam splitter, and then reflected by an artificial deformed mirror where the pupil ($\Phi = 12mm$) is located. Therefore, an unknown aberration is introduced by this mirror. The light beam is split into two beams by another beam splitter after passing through imaging lens L2 ($f = 300mm, \Phi = 50.8mm$). As the two beams reach the CCD (Andor Zyla 4.2) through different optical paths, the focused and defocused images can be recorded simultaneously, in which the introduced defocused distance is 1λ PV. A focused image is used at a high light level without aberration to provide an approximation of the pristine object, and a focused image is degraded using fixed aberrations at a high light level to evaluate noise levels. Poisson distributed noise is notable at low light levels, and thus, noisy images are obtained by reducing light intensity, as shown in Fig. 5 (Row 1), which corresponds to noise levels of 43.1, 36.6, 30.7, 26.8, and 22.6 dB in terms of PSNR.

The experimental results are in good agreement with the simulation results. Our approach consistently achieves good performances both in terms of subjective visual perception and SSIM at all noise levels. Images restored using the traditional PD technique, as shown in the second row in Fig. 5, include massive grains that cause varying degrees of destruction to the details. Distinguishing the object from the background becomes difficult because the edges are buried into a strong background as noise level increases. The bottom row provides good visual effects with few grains and a relatively high contrast. The reconstructed object can be recognized easily given its weak background and well-preserved details even at the highest noise level. Except for the subjective visual perception, the images reconstructed using the improved PD exhibit considerable improvement in terms of SSIM, as shown in Fig. 6, in a same trend as the simulation results. In the case of the traditional PD, SSIM drops dramatically as noise level rises. The overall decline range of SSIM is 42.2% for the traditional PD technique and only 5.2% for the improved PD technique. The experiments show that the results obtained using the improved PD technique exhibit higher accuracy and precision. The PD technique is clearly incapable of suppressing noise, but instead, is sensitive to it. Making full use of all the image data is a merit, as well as a demerit, of the PD technique. Each noise datum is regarded as useful information to be calculated, which causes the rapid decline of the estimated phase aberration precision and quality of the restored objects. The performance of the improved PD technique applied to images of noisy systems is verified by the aforementioned experiments. This method may be used in various domains, such as in the measurements of intrinsic aberrations and compensations for atmospheric turbulence.

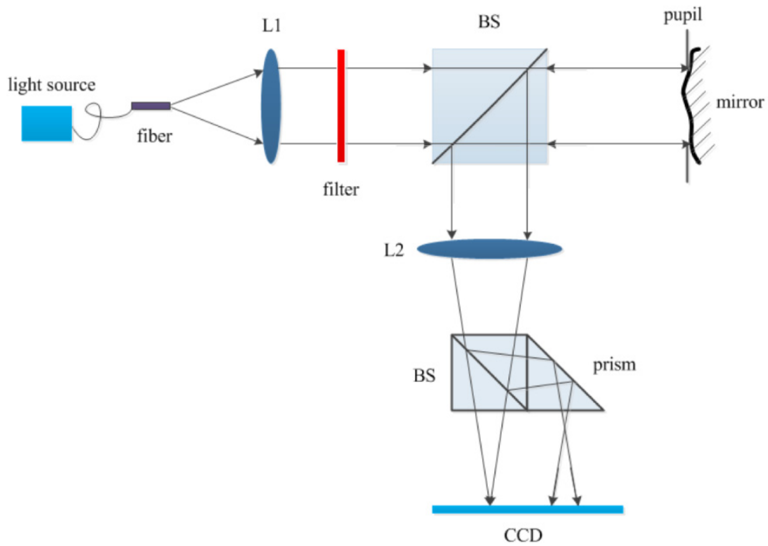

Fig. 4. Optical layout of the proposed verification experiment

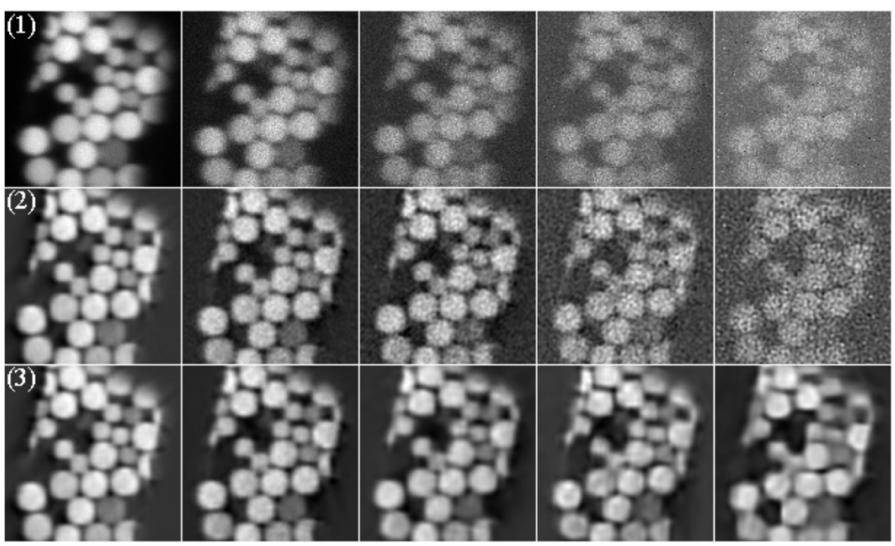

Fig. 5. Row 1: focused images captured by CCD. Row 2: images restored using the traditional PD technique. Row 3: images reconstructed using the improved PD technique.

Optics EXPRESS

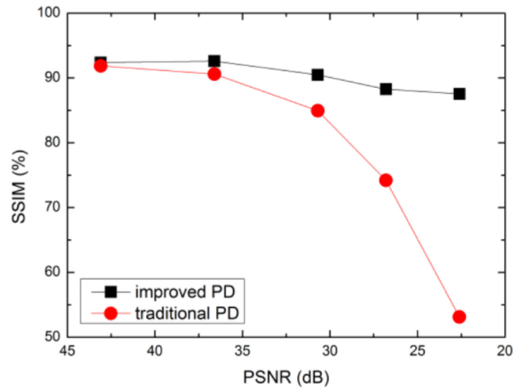

Fig. 6. Experimental results: SSIM of the reconstructed images as a function of the PSNR of the noisy focused images.

4. Conclusion

In this study, we propose an effective improvement on the PD technique to weaken the influence of Poisson noise. The poor performance of the traditional PD technique at low photon counts is improved by combining this technique with a denoising strategy based on the BM3D algorithm. The performance of the improved PD technique is confirmed by comparing the results of simulations and experiments. The RMSE of phase estimates on synthetic data in the case of the improved method is approximately 40% lower than that in case of the traditional PD technique across noise levels ranging from 58.7 dB to 18.8 dB while Strehl Ratio is 0.879, 0.499, and 0.204, respectively. The overall decline range of SSIM for the improved PD technique is less than 9%. However, SSIM drops by over 49% for the traditional PD. The experiments results are in good agreement with the simulation results. All the results demonstrate that the improved algorithm provides a valuable approach for the wavefront sensing technique to work under noisy conditions. The improved PD technique is useful in noisy active and adaptive optic systems.

Funding

Natural National Science Foundation of China (NSFC) (61475152, 61405194); Foundation of State Key Laboratory of Applied Optics, Changchun Institute of Optics, Fine Mechanics and Physics, Chinese Academy of Sciences.